Weather Radar Monitoring using the Sun

Iwan Holleman and Hans Beekhuis

Technical Report, KNMI TR-272, 2004

Contents

1 Introduction **5**

2 Detection of solar interferences **7**
2.1 Solar artifacts in reflectivity data 7
2.2 Automated detection of interferences 10
2.3 Attenuation correction 12
2.4 Overlap and azimuthal averaging 13
2.5 Corrected solar power 15

3 Position of the sun **17**
3.1 Celestial sphere and equatorial coordinates 17
3.2 Equatorial coordinates of the sun 18
3.3 Conversion to elevation and azimuth 20
3.4 Refraction correction 20

4 Power of the sun **23**
4.1 Solar spectrum 23
4.2 Solar flux monitor 24
4.3 Conversion of flux to received power 26

5 Analysis of solar interferences **27**
5.1 Scatter plot analysis 27
5.2 Numerical evaluation 28

6 Results **31**
6.1 Case 1: De Bilt radar 31
6.2 Case 2: Den Helder radar 33

7 Conclusions **37**

References **39**

Chapter 1

Introduction

In conjunction with the 81^{st} meeting of the American Meteorological Society a radar calibration workshop was organized by Paul Joe (MSC, Canada). This workshop was held on 13 and 14 January 2001 in Albuquerque, New Mexico, and about 35 presentations were given on various topics related to radar calibration. The use of the radio frequency radiation of the sun for off-line calibration of the alignment of the antenna and the sensitivity of the receiver was mentioned a number of times (Smith, 2001; Rinehart, 2001; Keeler, 2001; Crum, 2001; Tapping, 2001). Smith (2001) and Rinehart (2001) both discussed the use of the sun for measuring antenna gain patterns, but this is quite difficult because the sun is not a point target. The use of the sun for calibration of the alignment of the radar antenna was mentioned by Keeler (2001). Crum (2001) presented encouraging results of the receiver calibration of the entire NEXRAD radar network using the sun. Validation of the solar calibration method revealed that the obtained biases are consistent with field reports. Finally, Tapping (2001) from the Dominion Radio Astrophysical Observatory (DRAO) in Canada introduced the 10.7 cm solar flux monitor and detailed its use for calibration of antennas and receivers.

At the 31^{st} conference on radar meteorology, Darlington et al. (2003) showed that the antenna pointing of weather radars can be monitored on-line using unprocessed polar data from the operational scans. So the solar monitoring did not interfere with the operational use of the radar. Huuskonen and Hohti (2004) have presented similar results at the recent European Conference on Radar Meteorology and Hydrology (ERAD) and they showed that a single sunrise or sunset is sufficient to determine the antenna elevation pointing. At KNMI, Herman Wessels has previously used the solar artifacts in the operational echotop product to point out a 0.3 degree elevation bias of the radar in Den Helder.

In this technical report a tool for checking the antenna pointing and for on-line monitoring of the sensitivity of the radar receiver based on solar observations is presented. The monitoring tool does not interfere with the operational scanning of the weather radars: it merely analyzes the reflectivity volume scans which are produced in real-time. It is concluded that the potential of the "solar monitoring" tool is clearly demonstrated and that it should be consulted by the

maintenance staff on a daily basis. The outline of the remaining of the report is as follows:

- In chapter 2 it is demonstrated that solar interferences can be detected automatically in the reflectivity volume data from the operational weather radars.
- The motion of the sun along the celestial sphere is discussed in chapter 3 and the equations for calculation of the elevation and azimuth of the sun are given.
- In chapter 4 some details of the solar radiating spectrum are highlighted and the Dominion Radio Astrophysical Observatory (DRAO) which runs a solar flux monitoring program is introduced.
- A method to analyze the collected solar interferences and to extract quantitative information on the biases of the elevation and azimuth reading of the antenna and on the received solar power is described in chapter 5.
- In chapter 6 two cases are discussed which illustrate that the daily display of the analyzed solar interferences is a useful tool for monitoring the performance of the weather radars.
- In the last chapter the conclusions and recommendations for further application are made.

Chapter 2

Detection of solar interferences

In this chapter it is demonstrated that solar interferences can be seen in reflectivity volume data recorded operationally by weather radar and a method for automated detection of these interferences is proposed. Furthermore corrections of the received solar power for atmospheric attenuation and averaging losses are discussed.

2.1 Solar artifacts in reflectivity data

In the low-altitude reflectivity composite of KNMI, which is composed of data from the radars in De Bilt and Den Helder, artifacts due to interference from the sun are present on a regular basis. The artifacts occur around sunrise or sunset and they can be recognized in the image as spokes in the direction of one of the radars. Because of the relatively high threshold of 7 dBZ used by the KNMI radar displays, the artifacts are only observed when the sun's position is (almost) exactly in the direction of the radar antenna. In fact solar artifacts can be observed much more frequently in the raw polar volume data of the radars.

Figure 2.1 shows a so-called B-scope plot of polar reflectivity data of De Bilt recorded at 15:17 UTC on 2 February 2004 using an elevation of 7.5 degrees. The horizontal axis of the figure represents the range, the vertical axis represents the azimuth, and the color scale represents the observed reflectivity. The horizontal line of reflectivity extending over all ranges at an azimuth of 230.5 degrees is caused by interference from the sun. Note that this ray is averaged in tangential direction between 230 and 231 degrees azimuth by the radar processor. Because the sun is, in contrast to echoes from a pulsed weather radar, a continuous source of radio frequency radiation it is visible at all ranges. It is evident from figure 2.1 that the solar artifacts can easily be recognized in the polar reflectivity data and that their azimuth and elevation can be deduced, in this case 230.5 and 7.5 degrees, respectively.

In figure 2.2 a cross-section along the solar artifact, i.e., at an azimuth of 230.5 degrees in figure 2.1, is shown. The upper frame shows the observed reflectivity as a function of range. The characteristic range dependence of the solar interferences is clearly visible as a

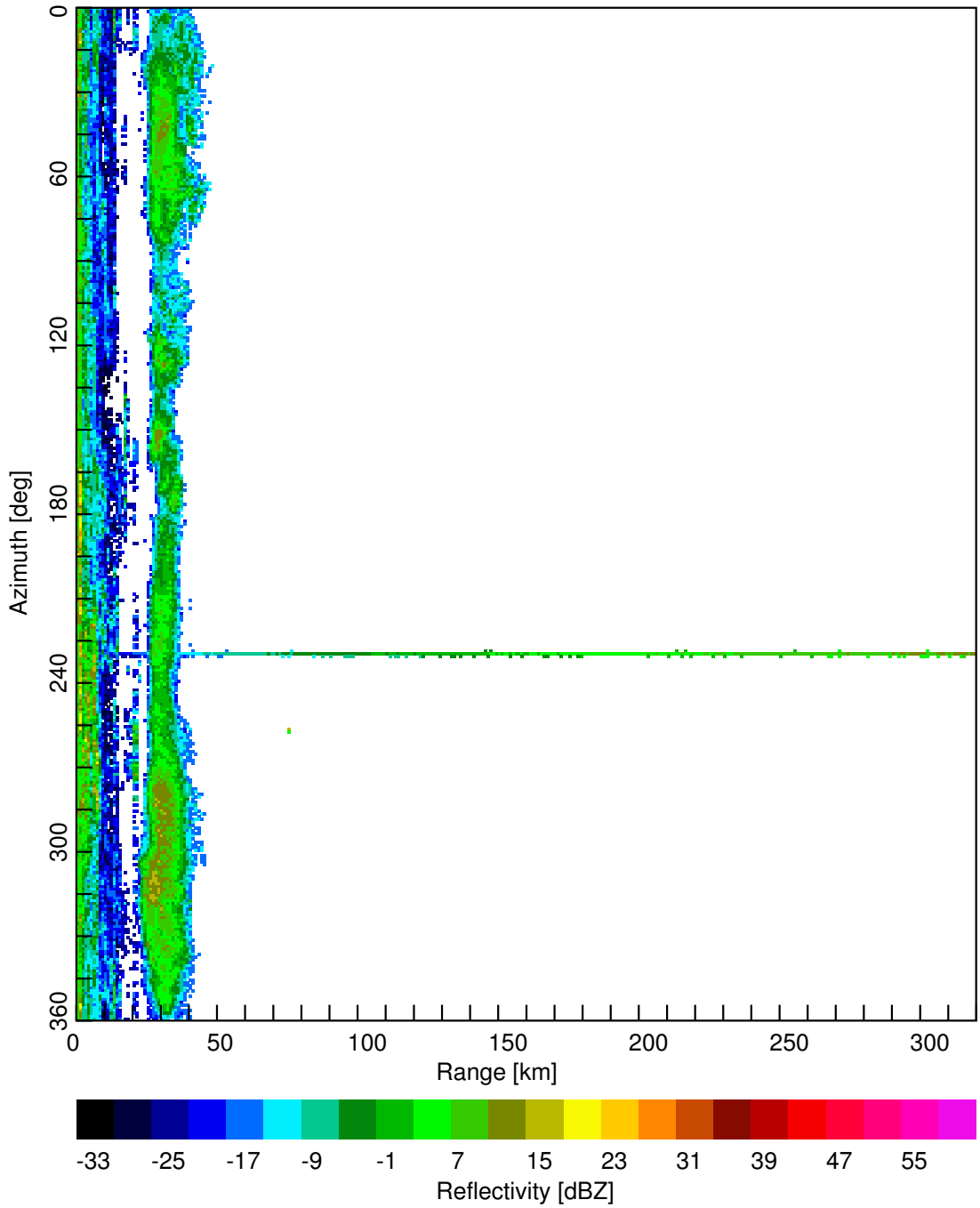

Figure 2.1: B-scope plot of polar reflectivity data of De Bilt recorded at 15:17 UTC on 2 February 2004 using an elevation of 7.5 degrees. The interference of the setting sun is clearly visible at 230 degrees azimuth.

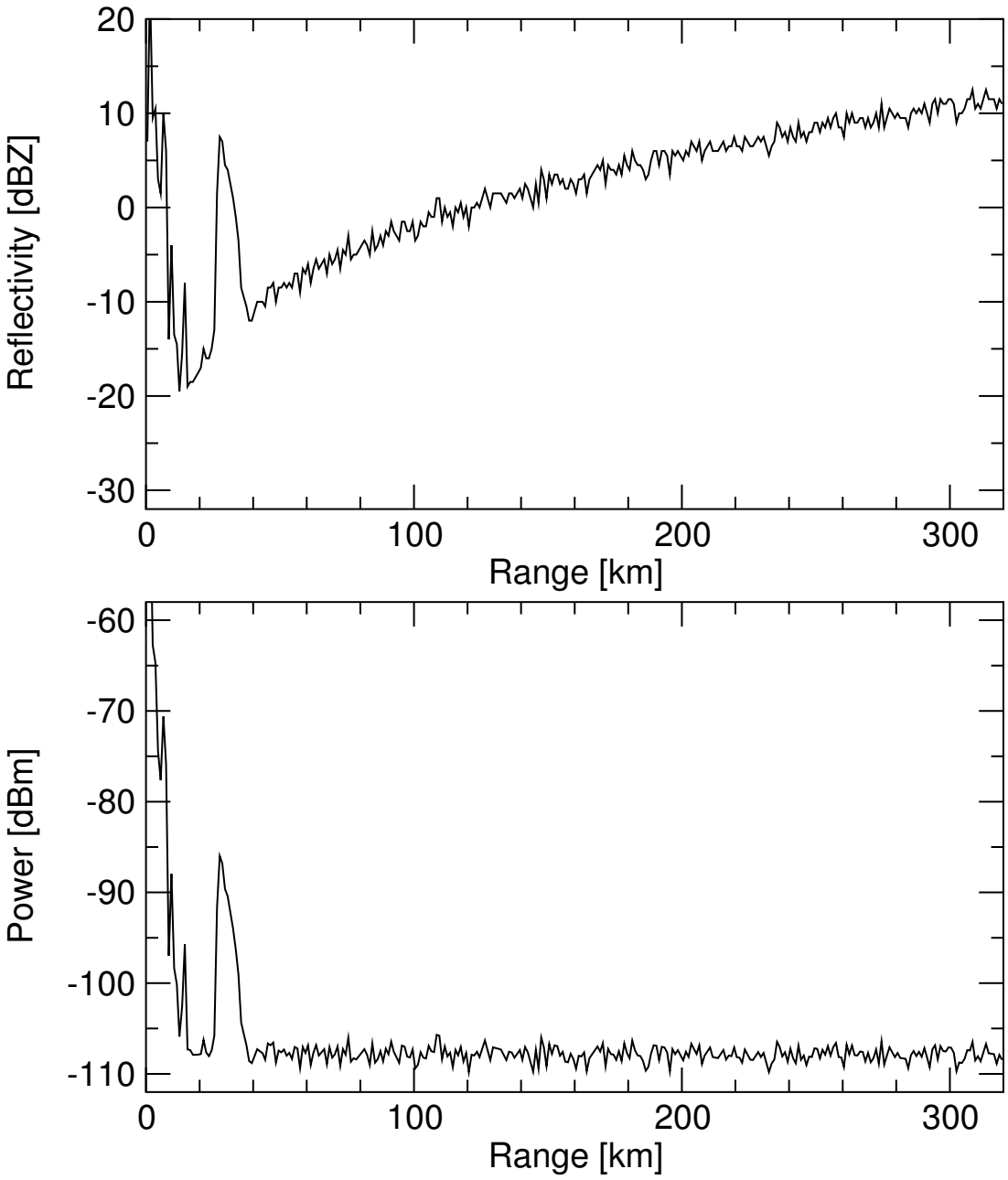

Figure 2.2: A-scope plot of the polar reflectivity data from figure 2.1 at an azimuth of 230.5 degrees, i.e., in direction of the sun, is shown in the upper frame. The typical range dependence of an interference from continuous source of radio frequency radiation is clearly visible. In the lower frame the range correction of the reflectivity values has been removed and the values have been converted to received power.

Table 2.1: This table lists the parameters that are used for the automated detection of solar interferences in the polar reflectivity data.

Parameter	Value
Minimum elevation	1.0 deg
Minimum range	200 km
Fraction of valid data	0.9
Maximum angular deviation	5 deg
Constant De Bilt	64.25 dB
Constant Den Helder	63.93 dB
Gaseous attenuation	0.008 dB/km

continuously increasing "background reflectivity". Only at ranges beyond roughly 250 km the signal from the solar interference exceeds the KNMI display threshold of 7 dBZ. The range dependence of the solar artifact, which originates from a continuous source of radio frequency radiation, is caused by corrections applied by the radar signal processor.

The received echo power is corrected by the radar signal processor for the geometrical $1/R^2$-reduction with range and for the attenuation due to scattering from molecular oxygen. The following equation is used by the processor to calculate the reflectivity in dBZ from the received power in dBm (SIGMET, 1998):

$$dBZ = dBm + 20\ {}^{10}\log R + 2\ a\ R + C \tag{2.1}$$

where R is equal to the range in km, a the one-way gaseous attenuation in dB/km and C the radar constant in dB. The applied values for the attenuation and radar constants are listed in table 2.1. Alternatively this equation can be used to recalculate the received power from the observed reflectivity. In the lower frame of figure 2.2 the received power calculated from the reflectivity data in the upper frame is plotted as a function of range. It is now clear that the observed artifact originates from a continuous source of radiation indeed. The received solar power of roughly -108 dBm is rather low, but it is well above the minimum detectable signal of the KNMI weather radars (< -109 dBm). In addition, it will be detailed below that the received solar power is attenuated by the averaging over 1 degree in azimuthal direction, and thus the received peak power was slightly higher.

2.2 Automated detection of interferences

For a numerical evaluation of the solar interferences an automated detection procedure of these interferences in polar reflectivity data is a prerequisite. It has been shown in the previous section

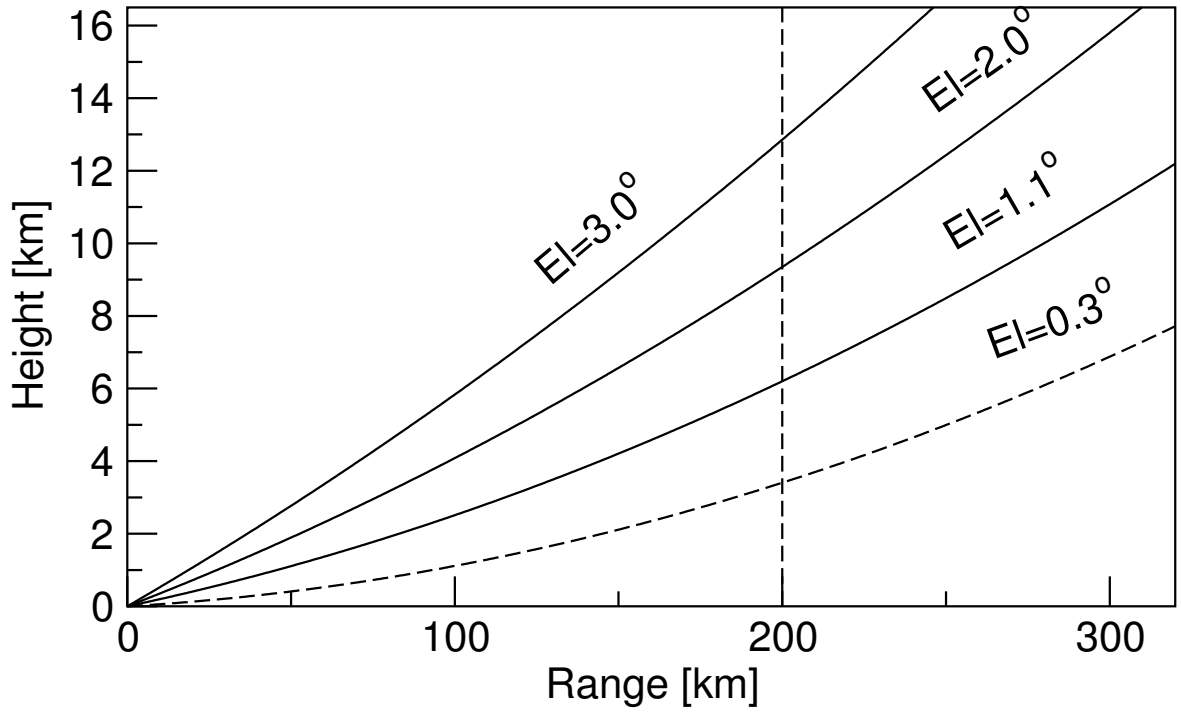

Figure 2.3: This figure shows the calculated height of the radar beam as a function of range for the 4 lowest elevations used by the KNMI radars. The minimum range used for identifying solar interferences is marked by the vertical dashed line. The lowest elevation is dashed because it is excluded from the analysis.

that the solar interferences give rise to very distinct artifacts in the polar data. Especially their extension to long ranges can be utilized for an automated detection procedure of the solar artifacts. In figure 2.3 the calculated height of the radar beam as a function of range for the 4 lowest elevations used by the KNMI radars is shown. It is evident from this figure that especially at the 3 highest elevations the radar beam gains height rapidly and that it, therefore, will overshoot precipitation at longer ranges. The presence of a consistent signal at long ranges, i.e., beyond 200 km, is the main signature for identification of solar interferences.

During the automated detection a polar volume of reflectivity data is scanned ray-by-ray. Only polar data recorded above a certain minimum elevation of typically 1 degree are considered. For each ray the number of range bins with valid reflectivity data, i.e., a reflectivity higher -31.5 dBZ, beyond a certain minimum range (default 200 km) is counted. A solar interference is detected when:

- the fraction of valid range bins is higher than a certain threshold value of typically 0.9, and

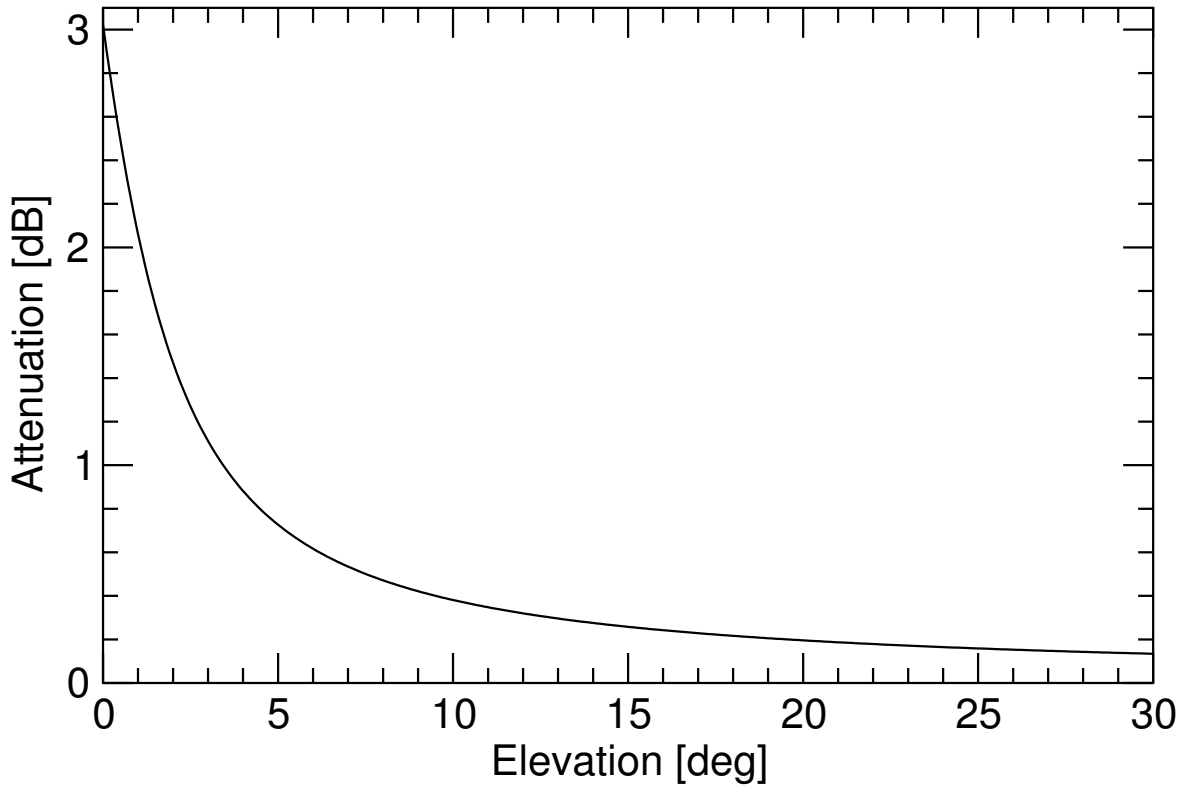

Figure 2.4: This figure shows the calculated attenuation between the radar antenna and the top of the atmosphere due to molecular attenuation as a function of elevation.

- the corresponding azimuth and elevation are close (default within 5 degrees) to the calculated position of the sun.

For each detected solar interference, the date and time, the calculated solar azimuth and elevation, and the observed azimuth, elevation, and solar power are stored. The time at which polar data is recorded is crucial and it should be accurate within 10-20 seconds for obtaining reliable results. Because the volume data files from the Gematronik Rainbow system (Gematronik, 2003) do not contain the exact time of each recorded elevation, a table with time offsets is used to calculate the time of a recorded elevation from the time stamp of the volume dataset. The parameters used for the automated detection of the solar interferences are listed in table 2.1.

2.3 Attenuation correction

It has been detailed in section 2.1 that during the reconversion of the observed reflectivity to the received power the range-dependent attenuation correction is removed. For comparison of the

received solar power with a reference, the received power has to be corrected for the gaseous attenuation between the radar antenna and the top of the atmosphere. This correction depends on the length of the path through the atmosphere and thus on the elevation of the antenna.

Using the commonly applied $4/3$ earth's radius model (Doviak and Zrnić, 1993), the range r from the radar can be written as a function of the elevation el and the height z:

$$r(z, el) = R_{43}\sqrt{\sin^2 el + \frac{2z}{R_{43}} + \frac{z^2}{R_{43}^2}} - R_{43}\sin el \tag{2.2}$$

where R_{43} is the $4/3$ radius of the earth. For the calculation of the gaseous attenuation between the radar antenna and the top of the atmosphere, the atmospheric density as a function of height is assumed to be constant and non-zero up to the "equivalent height" z_0 and zero above. The gaseous attenuation is then be approximated by:

$$A_{gas}(el) \simeq a \cdot r(z_0, el) \tag{2.3}$$

where a is the one-way gaseous attenuation at ground level in dB/km. The error due to this equivalent height approximation compared to using an exponential decaying density according to the 1976 US Standard Atmosphere is less than 8% for $el = 0$. The equivalent height z_0 of the atmosphere is chosen such that the integrated density is conserved:

$$z_0 \equiv \frac{1}{n_0}\int_0^\infty n(z)\, dz = \frac{p_0}{n_0 g} = \frac{RT_0}{g} \tag{2.4}$$

where the hydrostatic equation (Holton, 1992) has been used to evaluate the integral. Symbol T_0 represents the atmospheric temperature at ground level, R the gas constant, and g is the gravitation constant. Using the temperature from the 1976 US Standard Atmosphere ($T_0 = 288.15$ K), an equivalent height of 8.4 km is obtained. In figure 2.4 the gaseous attenuation between the antenna and the top of the atmosphere is plotted as a function of elevation using equation 2.3. It is evident from the figure that attenuation between the antenna and the top of the atmosphere is significant (up to 3 dB) at low elevations. The values of the parameters used to calculated the attenuation correction are listed in table 2.2.

2.4 Overlap and azimuthal averaging

The observed solar power is attenuated by the (imperfect) overlap with antenna sensitivity pattern function and the averaging of received power while the radar antenna is rotating along the azimuth. The overlap and averaging attenuation can be estimated by a simple 1-dimensional model. The solar power S and antenna pattern f as a function of azimuth az are approximated by Gaussian distributions:

$$S(az) \;=\; \sqrt{\frac{4\ln 2}{\pi\Delta_s^2}}\exp\left(\frac{-4\ln 2\; az^2}{\Delta_s^2}\right) \tag{2.5}$$

Table 2.2: This table lists the parameters that are used for the correction of the received solar power.

Parameter	Value
Receiver losses De Bilt	3.05 dB
Receiver losses Den Helder	2.34 dB
Gaseous attenuation	0.008 dB/km
Equivalent height of atmosphere	8.4 km
$4/3$ earth's radius	8495 km
Solar width, Δ_s	0.54 degrees
Radar beam width, Δ_r	0.95 degrees
Azimuthal bin size, Δ	1.0 degrees

$$f(az) \;=\; \exp\left(\frac{-4\ln 2\; az^2}{\Delta_r^2}\right) \tag{2.6}$$

where Δ_s and Δ_r are the beam widths of the sun and the radar antenna, respectively. For the solar power, a boxcar function would be more appropriate but this severely hampers an analytical evaluation of the overlap and averaging losses. It can be shown that for a perfect overlap between the sun and the antenna, i.e., $x = 0$ (see below), the error due to this approximation is less than 7%. The prefactors have been chosen such that the integrated solar power and the maximum transmission of the radar antenna are equal to 1. The fraction of the solar power received by the radar antenna A can be approximated by:

$$A(x) = \int S(az)\cdot f(az+x)\; daz = \sqrt{\frac{\Delta_r^2}{\Delta_s^2+\Delta_r^2}}\exp\left(\frac{-4\ln 2\; x^2}{\Delta_s^2+\Delta_r^2}\right) \tag{2.7}$$

where x is the azimuthal deviation between the radar antenna and the sun. Even when the overlap between the sun and the radar antenna is perfect ($x = 0$), the received solar power is attenuated due to the antenna sensitivity pattern. The effect of averaging in azimuthal direction by the radar processing can be estimated by A_{avg}:

$$A_{avg} = \frac{1}{\Delta x}\int_{-\Delta x/2}^{\Delta x/2} A(x)\; dx = \sqrt{\frac{\pi\Delta_r^2}{4\ln 2\;\Delta x^2}}\;\mathrm{erf}\left(\frac{\sqrt{\ln 2}\;\Delta x}{\sqrt{\Delta_s^2+\Delta_r^2}}\right) \tag{2.8}$$

where Δx is the azimuthal bin size and "erf" represents the error function (Press et al., 1992). Using a solar beam width of 0.54 degrees, a radar beam width of 0.95 degrees, and an azimuthal bin size of 1.0 degree, an overlap and averaging attenuation of 1.39 dB is found. The values of the parameters used to calculated this attenuation are listed in table 2.2.

2.5 Corrected solar power

For comparison of the received solar power with reference observations it is a prerequisite that the power is corrected for all attenuation between the receiver and the top of the atmosphere. Two sources of attenuation have been discussed in the previous sections, and the third source of attenuation is caused by the receiver losses. Using these known sources of attenuation the corrected received solar power $d\hat{B}m$ can be written as:

$$d\hat{B}m = dBm + A_{avg} + A_{gas}(el) + A_{Rx} \tag{2.9}$$

where dBm is the uncorrected received power calculated using equation 2.1 and A_{Rx} represents the receiver losses including the dry radome attenuation. The values of the parameters used to calculated the corrections are listed in table 2.2.

Chapter 3

Position of the sun

For the analysis of the solar inferences in the polar reflectivity data, the position of the sun at a given location and date/time needs to be known. This chapter describes the procedure that is used to calculate the elevation and azimuth of the sun.

3.1 Celestial sphere and equatorial coordinates

Due to the daily rotation of the earth and different viewing angles, the position of an object in the sky depends on the date/time and the geographical longitude and latitude. The position of these objects as seen from earth is, therefore, described using the coordinates on the so-called celestial sphere. In this coordinate system dependencies due to the daily rotation of the earth and to the latitude and longitude of the observer are removed, and thus providing viewer independent coordinates of objects in the sky, like the sun. A schematic drawing of the celestial sphere and the equatorial coordinate system is presented in figure 3.1.

The angles and plane which make up the celestial sphere and the equatorial coordinate system are defined as follows (Carroll and Ostlie, 1996):

Celestial equator The plane passing through the Earth's equator and extending to the celestial sphere is called the celestial equator.

Declination δ The declination is the equivalent of the latitude in the geographical coordinate system and it is measured in degrees north from the celestial equator.

Vernal equinox Υ The sun crosses the celestial equator twice a year. The first annual crossing of the sun through the celestial equator is called the vernal equinox (around 20 March), and the second crossing is called the autumnal equinox (23 September).

Right ascension α The right ascension is the equivalent of the longitude in the geographical coordinate system and it is measured eastward in hours along the celestial equator from the vernal equinox.

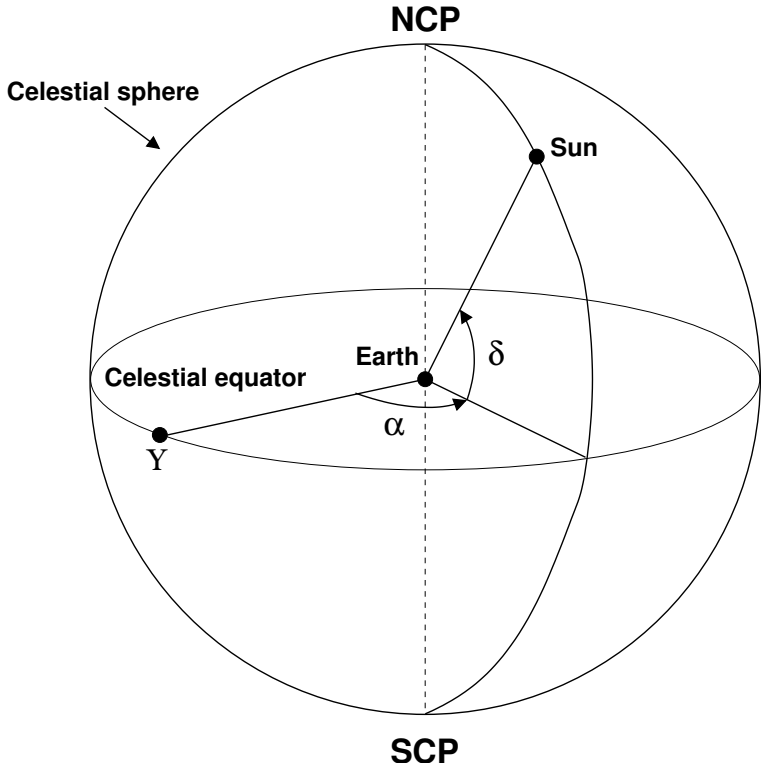

Figure 3.1: The figure shows the celestial sphere and the equatorial coordinate system. This figure is inspired by Carroll and Ostlie (1996).

The position of the sun on the celestial sphere is described by the declination δ and the right ascension α (see figure 3.1), i.e, the equatorial coordinates.

3.2 Equatorial coordinates of the sun

The equatorial coordinates of the sun (α,δ) depend on the motion of the earth around the sun. According to the First law of Johannes Kepler, the motion of the earth around the sun is described by an ellipse. The position of the earth in its elliptical orbit is described by an angle θ. The change of this angle per unit of time is not constant in time, but depends on the distance between the earth and the sun. This important fact is known as the Second law of Kepler. The angle θ in degrees of the earth in its orbit around the sun as a function of day number n is given by (WMO, 1996):

$$\theta(n) = 280.460 + 0.9856474 \cdot n + 1.915 \sin\bar{\theta} + 0.020 \sin 2\bar{\theta} \quad (3.1)$$

$$\bar{\theta} = 357.528 + 0.9856003 \cdot n \quad (3.2)$$

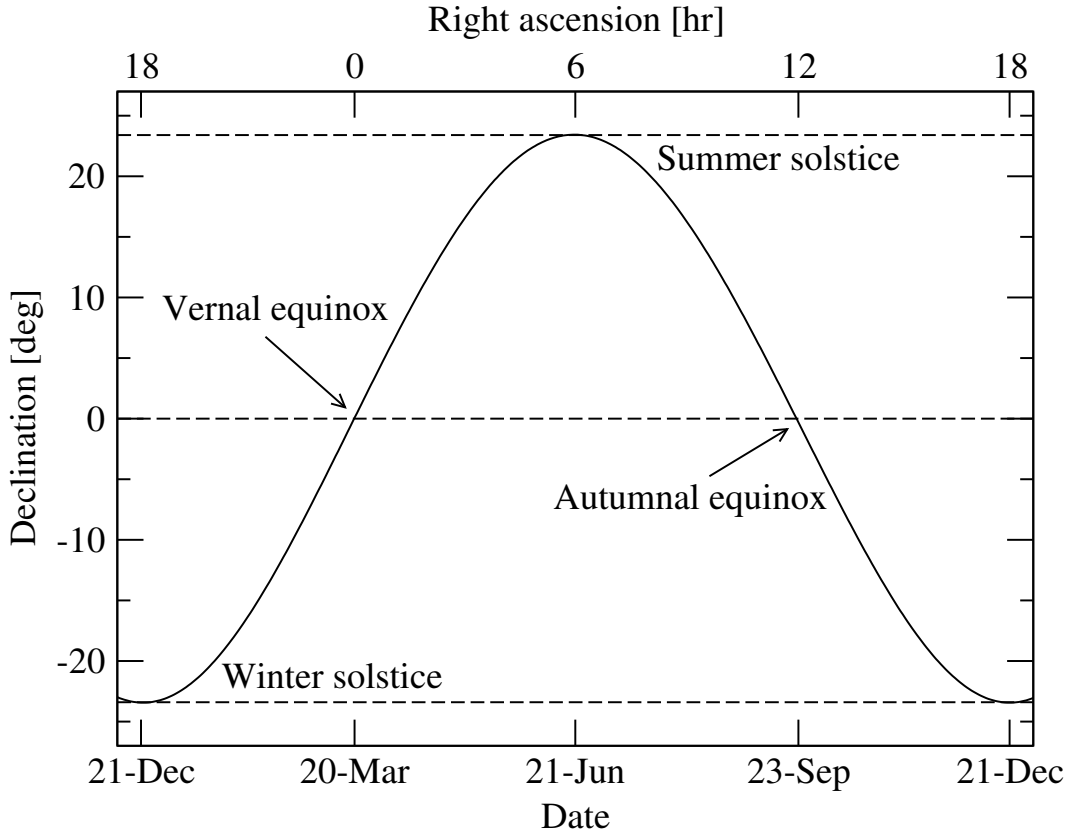

Figure 3.2: The figure shows the annual path of the sun across the celestial sphere. This figure is inspired by Carroll and Ostlie (1996).

where the day number n is defined as the number of days since 1 January 2000 or alternatively: $n = julday - 2451545$ where $julday$ is the Julian day number.

Apart from the angle θ one also needs the angle between the polar axis and the plane of earth's orbit around the sun (obliquity) to calculate the equatorial coordinates of the sun. The dependence of the obliquity δ_0 in degrees as a function of day number is (WMO, 1996):

$$\delta_0(n) = 23.439 - 4 \cdot 10^{-7} n \tag{3.3}$$

and it thus can be considered constant for our application. Using the previous equations for the orbit angle θ and the obliquity δ_0, the right ascension and declination can be calculated using a straightforward rotation:

$$\tan \alpha(n) = \cos \delta_0 \tan \theta \tag{3.4}$$

$$\sin \delta(n) = \sin \delta_0 \sin \theta \tag{3.5}$$

where the right ascension α is usually measured in hours and the declination δ in degrees. The declination as a function of the right ascension or the annual path of the sun across the celestial

sphere is depicted in figure 3.2. The elevation and azimuth of the sun can be calculated from the equatorial coordinates.

3.3 Conversion to elevation and azimuth

For conversion of the right ascension and declination on the celestial sphere to the actual elevation and azimuth of the sun, the local latitude ϕ and longitude λ, and the current hour angle of the sun are needed. The hour angle ha is defined as the difference between the celestial object (the sun in our case) and the local longitude (Carroll and Ostlie, 1996). The hour angle of the sun is given by (WMO, 1996):

$$ha = 6.697375 + 0.0657098242 \cdot n + hh + (\lambda - \alpha)/15 \tag{3.6}$$

where hh is the current UTC time in (fractional) hours and ha is measured in hours.

Using the laws of spherical trigonometry, the elevation el of the sun can be calculated from right ascension and declination:

$$\sin el = \sin\phi \sin\delta + \cos\phi \cos\delta \cos ha \tag{3.7}$$

where elevations between -90 and $+90$ degrees are allowed and negative elevations naturally indicate night time. Similarly, an equation for the tangent of the azimuth az of the sun can be deduced:

$$\tan az = \frac{-\sin ha}{\cos\phi \tan\delta - \sin\phi \cos ha} \tag{3.8}$$

where azimuths between 0 and 360 degrees are allowed.

3.4 Refraction correction

The radiation of the sun is refracted during its propagation through the atmosphere due to the change of refractive index with altitude. Because the atmospheric density is monotonically decreasing with increasing altitude, refraction always makes that the sun is apparently at a higher elevation. The effect of refraction can be described by the following equation (Sonntag, 1989):

$$el_a = el + \varrho(el, p, T) \tag{3.9}$$

where el_a is the apparent elevation and ϱ is the refraction as a function of the true elevation el, pressure p, and temperature T at ground level.

Many different equations have been deduced to approximate the refraction of the radiation from the sun or other stars as a function of elevation. Sonntag (1989) has optimized a straightforward equation for the refraction using tabulated values for the refraction as a function of

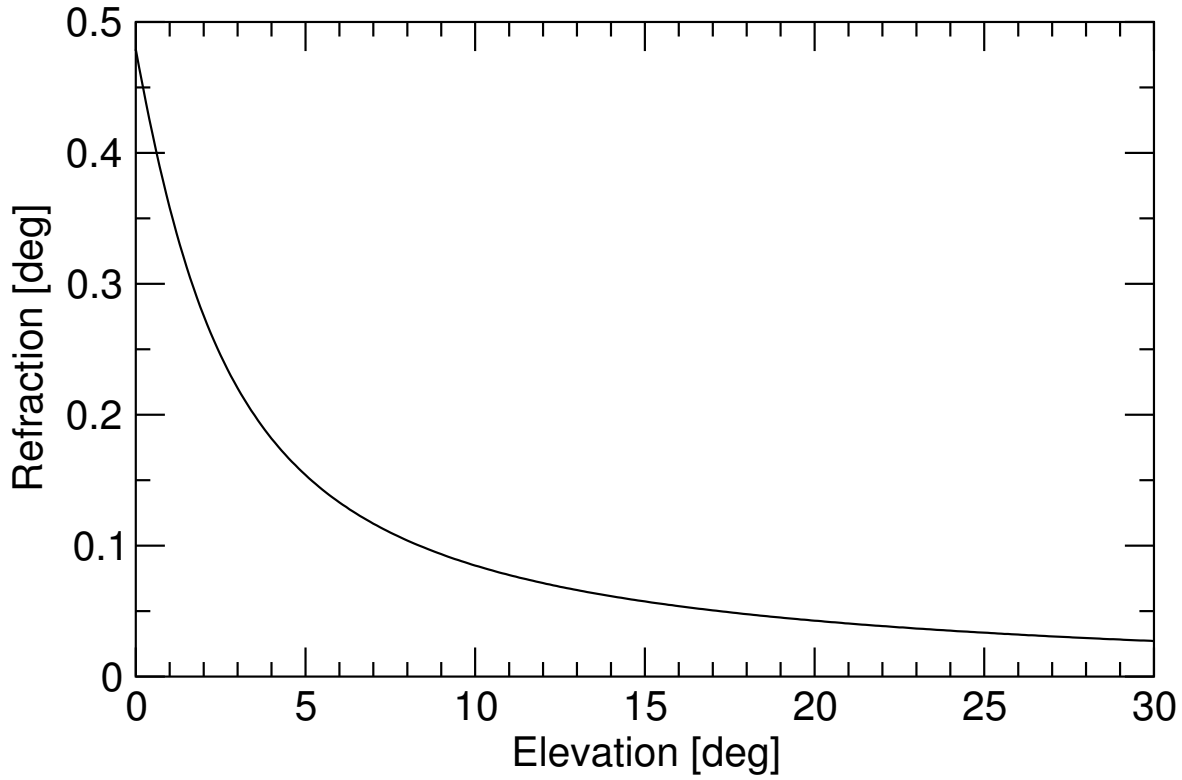

Figure 3.3: This figure shows the calculated refraction of the solar radiation as a function of the true elevation for T=288.15 K and p=1013.25 hPa (1976 US Standard Atmosphere).

pressure and temperature:

$$\varrho(el, p, T) = \frac{0.0045\, p}{T \tan[el + 8.0/(el + 4.23)]} \tag{3.10}$$

where ϱ and el are measured in degrees, and the temperature T and pressure p in Kelvin and hPa, respectively. The calculated refraction as a function of the true elevation is plotted in figure 3.3. The calculated refraction of the sun is maximum at zero elevation, but never exceeds 0.5 degrees. Note that this calculated refraction is optimized for visible light, but similar refraction is expected for radio-frequency radiation.

Chapter 4

Power of the sun

For an absolute check of the calibration of the weather radar receiver using the detected solar interferences information on the solar flux at C-band is a prerequisite. In this chapter some details of the solar radiation spectrum are highlighted and a Canadian solar flux monitoring station is introduced. Finally, equations for estimation of the C-band power received by the weather radar from the solar flux monitoring data are presented.

4.1 Solar spectrum

For an absolute calibration of the radar receiver, information on the solar flux at C-band is required. The surface of sun approximately radiates as a black body with an effective temperature of 5770 K (Carroll and Ostlie, 1996). Using this information the approximate solar spectrum can be calculated using the law of Max Planck for the radiation intensity from a black body as a function of wavelength (Carroll and Ostlie, 1996).

In figure 4.1 the calculated solar spectrum is shown on a log-log plot. The vertical axis represents the calculated solar flux in so-called Solar Flux Units (sfu) defined as 10^{-22} W/m^2/Hz and the horizontal axis represents the frequency of the radiation in GHz. A solar solid angle of 6.85×10^{-5} sterad is used for the calculation of the solar flux as received on earth. The log-log plot is chosen in order to facilitate a comparison of the fluxes in the radio frequency part (indicated by "C-Band") and the visible part (indicated by "Visible") of the spectrum. The visible part of the spectrum for humans is rather close to the peak of the solar spectrum. It is evident from the figure that the solar flux at C-band is about 9 orders of magnitude smaller than that in the visible part of the spectrum.

Because the radio frequency region is so far in the tail of the black body spectrum of the sun and the effective temperature is mainly determined by the visible radiation, the C-band intensity is not accurately described by the theoretical spectrum of figure 4.1. In addition, the radio frequency intensity of the sun varies strongly with the phase of the solar activity cycle and the presence of "hot spots" on the sun. An absolute calibration of the received C-

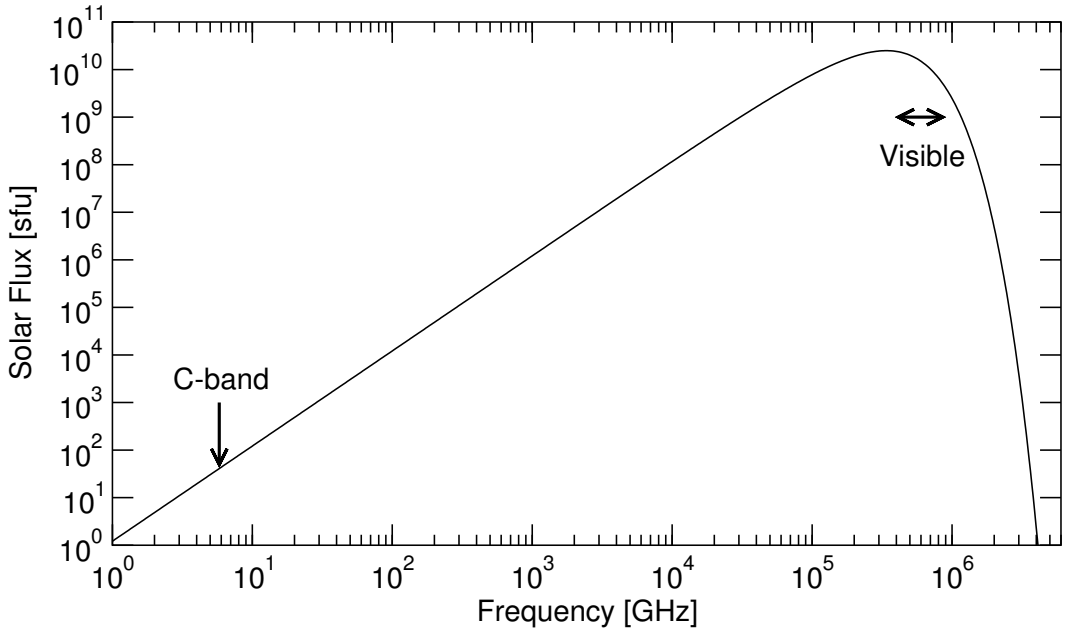

Figure 4.1: The calculated spectrum of the sun using a black body temperature of 5770 K.The spectrum is displayed on a log-log plot in order to facilitate comparison of the intensities in radio frequency and visible radiation.

band radiation using the sun can, therefore, only be done using observations from a reference monitoring station.

4.2 Solar flux monitor

The solar flux at a wavelength of 10.7 cm (S-band) is continuously monitored at the Dominion Radio Astrophysical Observatory (DRAO, `www.drao.nrc.ca`) in Canada. This observatory is located at a site near Penticton, British Columbia, which enjoys extremely low interference levels at centimeter wavelengths (Tapping, 2001). Observations of the daily solar flux have started in 1946 and have continued to the present day. The current solar flux at 10.7 cm can be obtained from the website of the DRAO observatory:

`www.drao-ofr.hia-iha.nrc-cnrc.gc.ca/icarus/www/current_flux.shtml`

On this web page the current solar flux and the adjusted solar flux, corrected for changes in the distance between the sun and the earth, are refreshed each day at 23 UTC. Both solar flux numbers are corrected for the atmospheric attenuation at S-band. The system calibration is checked periodically using a dual-horn receiver and a calibrated noise source. In figure 4.2 a time series of more than 50 years of adjusted solar flux data recorded at the Dominion Radio

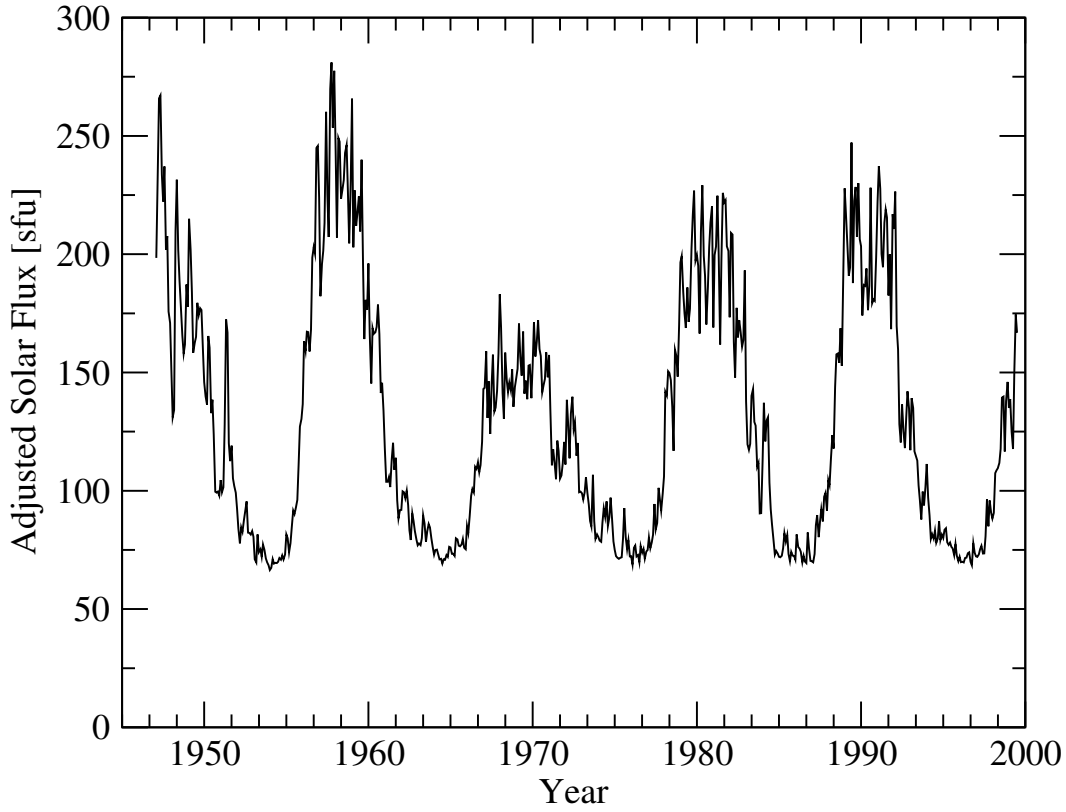

Figure 4.2: A time series plot of more than 50 years of 10.7 cm solar flux data recorded at the Dominion Radio Astrophysical Observatory (DRAO) in Canada. The solar flux is given in "solar flux units" equal to 10^{-22} W/m^2/Hz. These data are taken from the DRAO website: `www.drao.nrc.ca`.

Astrophysical Observatory is plotted. It is evident from the figure that the solar flux at this wavelength is far from being a constant: it varies roughly between 75 sfu and 275 sfu. The large fluctuations are due to the 10-13 year solar activity cycle and the small, noise-like fluctuations are due to shorter-time-scale variations of activity and the solar rotation with a period of about 30 days (Tapping, 2001).

The 10.7 cm (S-band) solar flux measurements can be applied to other frequencies with an accuracy of roughly 1 dB. This is possible because the solar emission at centimeter wavelengths can be divided into two distinct components: a steady base level and a superimposed slowly-varying component with a constant spectral shape. Tapping (2001) has used this property to derive an equation for the solar flux at certain wavelengths from the observed flux at 10.7 cm ($F_{10.7}$). The estimated solar flux at C-band (F_C) is given by:

$$F_C = 0.71 \cdot (F_{10.7} - 64) + 126 \tag{4.1}$$

Table 4.1: This table lists the parameters that are used for the conversion of the solar flux to received power.

Parameter	Value
Band width De Bilt	0.611 MHz
Band width Den Helder	0.617 MHz
Antenna dimensions	13.85 m^2

where the constants have been determined using observed flux densities at different wavelengths between 3 and 30 cm over two solar cycles and the fluxes are given in sfu. The estimated solar flux at C-band can be converted to the solar power received by a radar when the antenna dimensions and the receiver filter characteristics are known.

4.3 Conversion of flux to received power

As detailed above the solar flux observed at DRAO can be converted to the solar flux at C-band. From this solar flux, the maximum power that a weather radar can receive from the sun can be calculated when the antenna dimensions and the filter characteristics of the receiver are known. The estimated solar power p_{sun} in mW is given by:

$$p_{sun} = \frac{1}{2} \cdot 10^{-13} \cdot \Delta f \cdot A \cdot F_C \tag{4.2}$$

where Δf and A refer to the band width of the receiver in MHz and the area of the antenna in m^2, respectively. The factor $\frac{1}{2}$ is introduced because the sun is an unpolarized source while the radar antenna is sensitive to horizontal polarized radiation only. The antenna and receiver parameters are listed in table 4.1. The solar power estimated from the DRAO flux monitor should be compared to the corrected solar power from the weather radar observations as discussed in section 2.5.

Chapter 5

Analysis of solar interferences

By analysis of all reflectivity volume data produced by a weather radar, a number of solar interferences is collected each day around sunrise and sunset. In this chapter a method to analyze the collected interferences and to extract the elevation bias, the azimuthal bias, and the received solar power is described in detail. The method is based on a linear fit of the solar interference data to a model function representing the antenna beam shape.

5.1 Scatter plot analysis

The KNMI weather radars perform a 4-elevation reflectivity volume scan every 5 minutes and a 14-elevation reflectivity volume scan every 15-minutes. Each day about $20 - 35$ solar interferences are detected in the reflectivity volume data from the weather radar in De Bilt. The daily number of detected interferences depends on the season. i.e., on the ascension/descent rate of the sun, on the solar activity, on the scanning strategy, and on the sensitivity of the receiver. In figure 5.1 a scatter plot of the solar interferences collected during March 2004 by the radar in De Bilt is depicted. About 750 interferences ("all") have been collected during this month, and about 100 of them were classified as "strong", i.e., received solar power higher than -108 dBm. The vertical axis of the figure represents the difference between the observed antenna elevation (reading) and the calculated elevation of the sun, and the horizontal axis the same for the azimuth. The elevation and azimuth of the sun are calculated using the time stamp of the radar observation.

It is evident from figure 5.1 that the solar interferences are scattered over roughly 1 degree in both elevation and azimuthal direction. Furthermore it is evident that the strong solar interferences are scattered over a much smaller area, i.e., about 0.5 degrees in both directions, and that they are co-axial with "all" interferences. These solar interferences are evidently stronger because the sun and the radar antenna are better aligned in these cases. A small bias of the radar antenna in both elevation and azimuthal direction is exposed by the scatter plot analysis. This can be seen clearly from the large number of points in the lower-left quadrant of the scatter

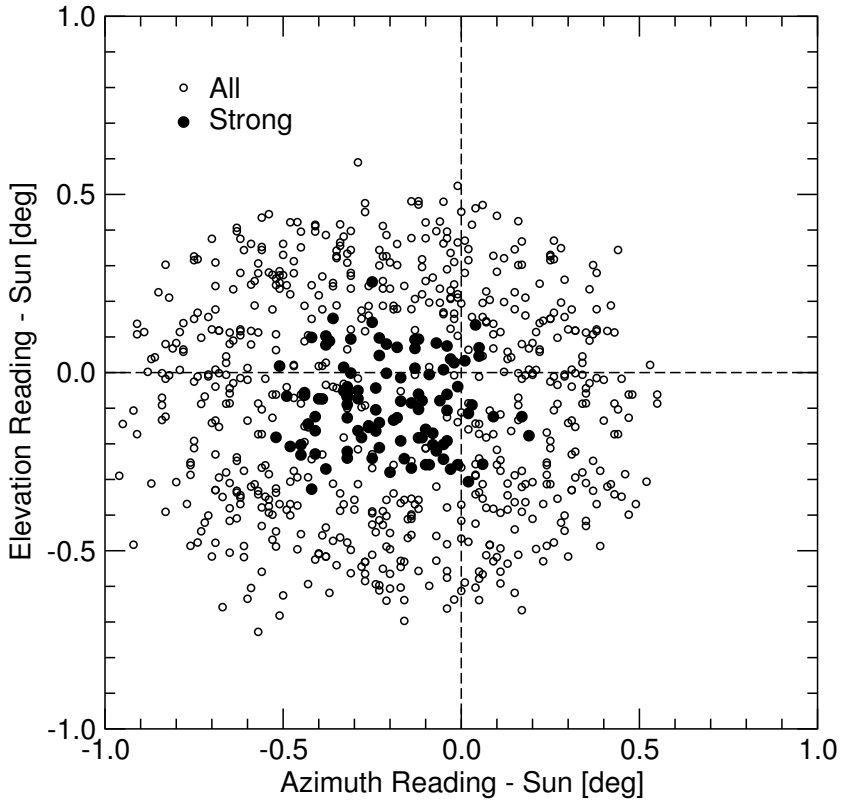

Figure 5.1: A scatter plot of the solar interferences collected by the weather radar in De Bilt during March 2004. The vertical axis represents the difference between the observed antenna elevation (reading) and the calculated elevation of sun, and the horizontal axis represents the same for azimuth. The open circles show "all" solar interferences, while the filled circles show the "strong" interferences with a solar power higher than -108 dBm.

plot. A close examination of the scatter plot reveals an antenna reading bias of approximately -0.1 degrees in elevation and of approximately -0.2 degrees in azimuth. In the next section a method for numerical evaluation of the collected solar interferences is presented which provides the elevation and azimuthal biases of the antenna reading and the maximum solar power received by the radar.

5.2 Numerical evaluation

The solar interferences with given elevation, azimuth, and received power collected over a predefined period can be analyzed using a numerical method and information on the biases of the antenna reading and the maximum solar power can be extracted. For this it is assumed that

the errors in the antenna reading of azimuth and elevation are mainly due to bias errors. It is hard to calibrate these angles within 0.1 degrees and sometimes the calibration is lost due to e.g. mechanical failure. The solar interferences can, therefore, be analyzed using the deviation between the observed antenna angle and the calculated solar angle. The azimuthal deviation x and elevation deviation y are defined as:

$$x = az_{read} - az_{sun} \tag{5.1}$$
$$y = el_{read} - el_{sun} \tag{5.2}$$

where (az_{read}, el_{read}) refer to the observed antenna angles and (az_{sun}, el_{sun}) to the calculated position of the sun. Before further analysis can be done, a shape for the solar power received by the antenna as a function of x and y needs to be assumed. In section 2.4 an equation for the received solar power as a function of the azimuthal deviation has been derived. Equation 2.7 shows that the received solar power as a function of x can be approximated by a Gaussian distribution. The received solar power $\tilde{p}(x, y)$ in mW is, therefore, approximated by the product of two Gaussian distributions:

$$\tilde{p}(x, y) \equiv \tilde{p}_0 \cdot \tilde{g}(x, x_0) \cdot \tilde{g}(y, y_0) \tag{5.3}$$
$$\tilde{g}(x, x_0) = \exp\left(\frac{-4 \ln 2 \, (x - x_0)^2}{\Delta^2}\right) \tag{5.4}$$

where $\tilde{p}_0$ represents the maximum solar power in mW, and x_0 and y_0 are introduced to account for the biases of the antenna reading in azimuth and elevation, respectively. The width Δ is determined by the antenna beam width and the diameter of the solar disk (see equation 2.7). The received power $\tilde{p}(x, y)$ is measured in units of dBm and thus the equation is converted accordingly:

$$p(x, y) = 10 \, {}^{10}\log(\tilde{p}) = p_0 + g(x) + h(y) \tag{5.5}$$

where the absence of a tilde indicates a power (factor) in dBm (dB). It is rather straightforward to see that the received solar power $p(x, y)$ can be written as:

$$p(x, y) = a \cdot x^2 + a \cdot y^2 + b_1 \cdot x + b_2 \cdot y + c \tag{5.6}$$

where it is important to note that this equation is linear in the parameters a, b_1, b_2, and c. The width Δ, the azimuth bias x_0, the elevation bias y_0, and the maximum solar power p_0 can be calculated from the linear parameters:

$$\Delta = \sqrt{-\frac{40 \, {}^{10}\log 2}{a}} \tag{5.7}$$
$$x_0 = -\frac{b_1}{2a} \tag{5.8}$$
$$y_0 = -\frac{b_2}{2a} \tag{5.9}$$
$$p_0 = -\frac{b_1^2 + b_2^2}{4a} + c \tag{5.10}$$

and naturally the width Δ can only be calculated when parameter a is negative.

The solar interferences collected over a certain period, typically a day, are analyzed using equation 5.6. Because this equation is linear in the parameters a to c, the solar interference data can easily be fitted to equation 5.6 by the least squares method (Press et al., 1992). The width (parameter a) is kept fixed during the fit in order to increase the stability of the fit and to reduce the number of fit parameters. The resulting values for parameters b_1, b_2, and c are then used to extract the biases and the maximum received solar power.

Chapter 6

Results

The solar interferences collected by the weather radars in De Bilt and Den Helder are analyzed on a daily basis. The results are displayed in real-time on the intranet of KNMI. In this chapter it will be illustrated that this display of the analyzed solar interferences is a useful tool for monitoring the performance of the weather radars.

6.1 Case 1: De Bilt radar

It has been detailed in the previous chapter that the collected solar interferences can be analyzed to obtain the azimuthal and elevation biases and the received solar power using a linear fit. In figure 6.1 the results of a daily analysis of the solar interferences collected by the radar in De Bilt between 27 March and 29 May 2004 are shown. The upper frame shows the number of solar interferences collected per day. During this period typically between 20 and 30 interferences are detected each day. The number of detected solar interferences depends on the season, i.e., the ascend/descend rate of the sun, on the solar activity, on the scanning procedure of the weather radar, and on the sensitivity of the radar receiver.

The middle frame of figure 6.1 shows the extracted biases of the azimuth (circles) and elevation (triangles) readings of the radar antenna. It is evident from the figure that the extracted elevation bias is slightly negative and fluctuates between -0.05 and -0.1 degrees. In order to have a correct height assignment of the radar observations, an elevation bias of maximum 0.1 degrees is acceptable for operational weather radars. So the bias of the antenna elevation reading of De Bilt is apparently within acceptable limits. In addition, the "noise" on the extracted elevation bias suggests that the random error on the elevation bias obtained from the solar interferences is less than 0.05 degrees. The extracted azimuth bias is also negative but somewhat larger than the elevation bias. It fluctuates between -0.1 and -0.3 degrees. For a weather radar the azimuth bias is less critical than the elevation bias. When the geographical referencing of the radar data has to be accurate within 1 km at 200 km range, the bias in the azimuth reading of the antenna must be less than 0.3 degrees. The random error on the azimuth

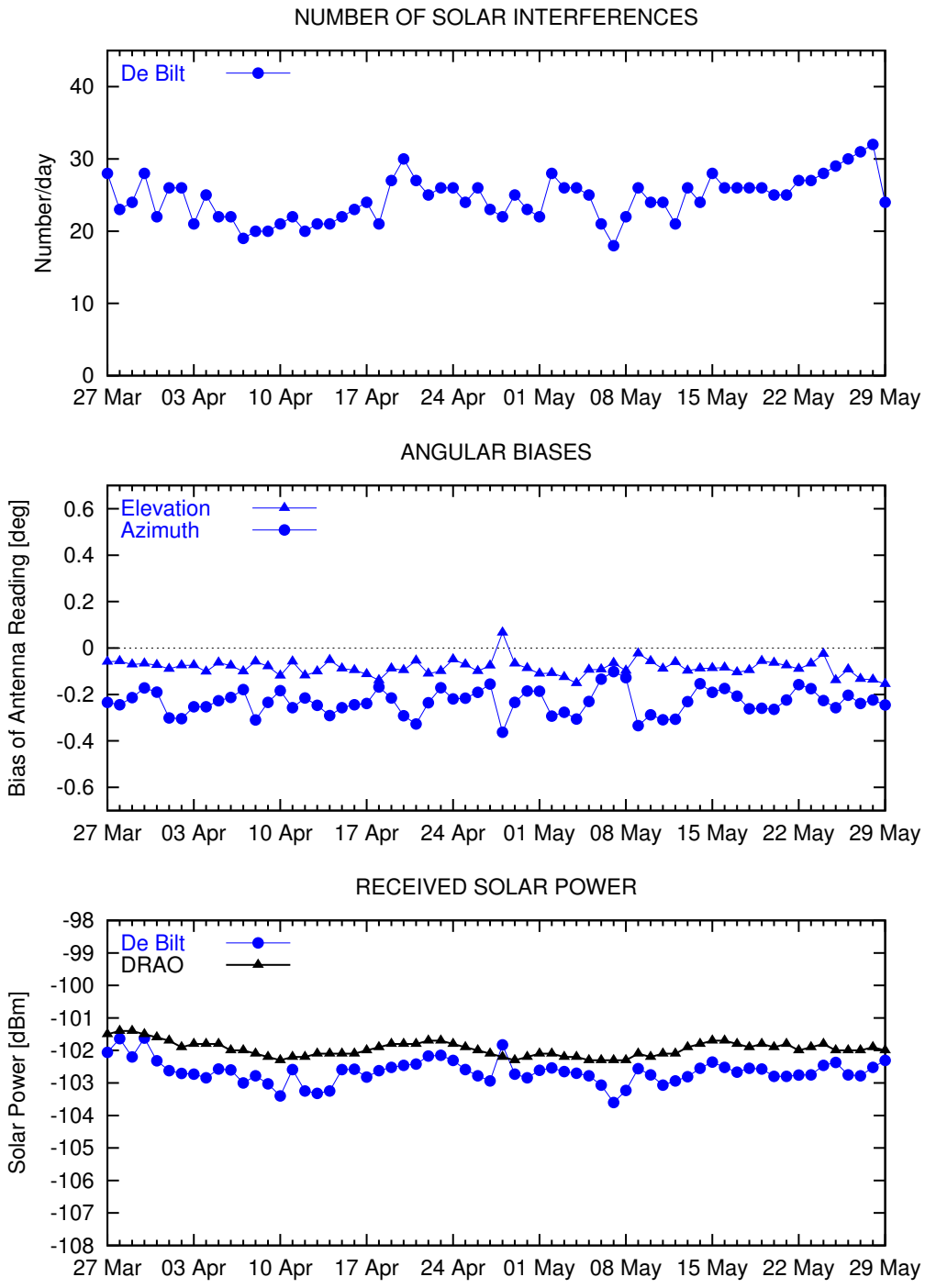

Figure 6.1: Example of the results of the daily analysis of the solar interferences detected by the radar in De Bilt between 27 March and 29 May 2004.

bias obtained from the solar interferences appears to be less than 0.1 degrees.

The received solar power by the radar De Bilt is shown together with the reference values from the Dominion Radio Astrophysical Observatory (DRAO) in the lower frame of figure 6.1. Equation 4.2 has been used to convert the DRAO solar flux to the reference solar power for the weather radar in De Bilt. It is evident from this figure that the power from the DRAO monitoring station and the received solar power by De Bilt agree within 1 dB. This excellent agreement suggests that the receiver of the weather radar in De Bilt is well calibrated. The random error on the received power obtained from the solar interferences appears to be a few tenths of dB only. A more careful examination of the figure reveals that the slow fluctuations in the DRAO reference signal are also present in the (smoothed) curve from De Bilt. On 28 April a clear outlier is observed both in the extracted biases and in the receiver solar power for the radar De Bilt. The residue of the fit is rather large for this day indicating that the solar interference data was rather noisy. This "noise" may be caused by the intensive rainfall around sunset on 28 April.

6.2 Case 2: Den Helder radar

In the previous section a "best case" has been discussed for the radar in De Bilt but it is not always like that. In this section the results of the daily analysis of the solar interferences collected by the radar in Den Helder over the same period (from 27 March till 29 May 2004) are presented and discussed. Figure 6.2 contains the results from the daily analysis for the radar in Den Helder. The upper frame again shows the number of solar interferences collected by the radar per day. During this period typically between 5 and 20 interferences are detected each day by the Den Helder radar, and this is significantly lower than what the De Bilt radar has detected during the same period (see figure 6.1). Because the data are collected over the same period and the scanning schemes of both radars are identical, this difference can only be explained by a lower sensitivity of the receiver in Den Helder.

In the middle frame of figure 6.2 the extracted biases of the azimuth and elevation readings of the radar antenna in Den Helder are shown. It is obvious that the biases of the antenna reading of Den Helder are not negligible and that the biases have jumped on at least two occasions during this period. The daily analyzes before 6 April indicate an elevation bias of -0.3 degrees and azimuth bias -0.6 degrees for this radar. During the annual maintenance of the radar, the antenna reading has been adjusted by $+0.3$ and $+0.5$ degrees in elevation and azimuth, respectively. The effect of this adjustment is clearly visible on 7 and 8 April as the elevation bias is now close to zero and the azimuth bias is reduced considerably. On 9 April it was discovered, however, that clock of the radar computer had an offset of about 108 seconds (!) because it had not been synchronized to the KNMI network clock for a long time. The clock of the radar computer has been synchronized manually on the same day and the automatic synchronization to the KNMI network clock was reestablished on 21 April. The effect of this (manual) synchro-

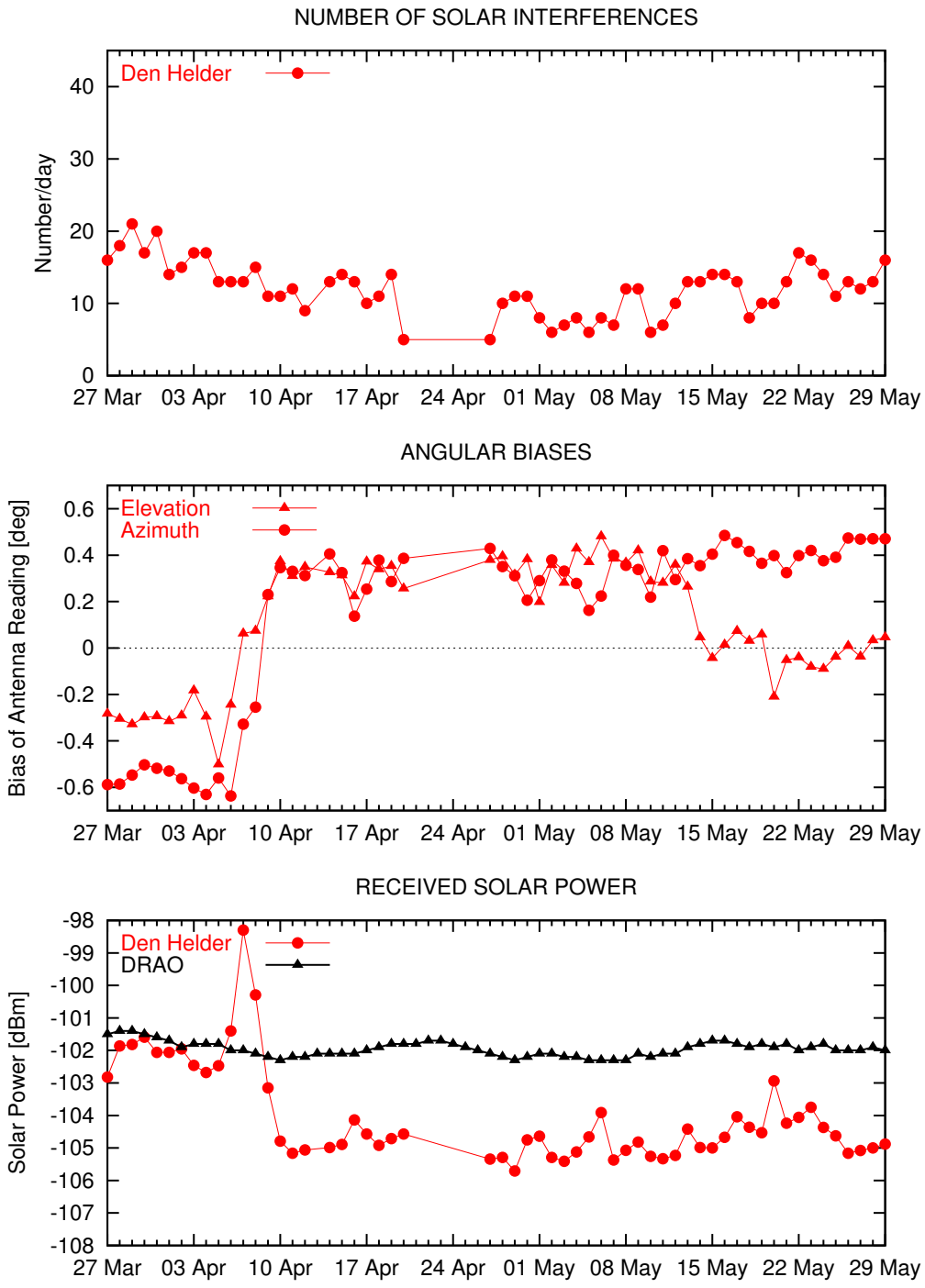

Figure 6.2: Example of the results of the daily analysis of the solar interferences detected by the radar in Den Helder between 27 March and 29 May 2004.

nization on the observed biases is evident: both the elevation and azimuth bias have increased to about $+0.4$ degrees. During a second visit to the radar in Den Helder on 13 May, the elevation reading of the antenna has been adjusted by -0.3 degrees, i.e., the previous adjustment has been undone. After this day no significant bias is observed for the elevation reading of the antenna in Den Helder. This example clearly illustrates that the time stamp of the detected solar interferences should be accurate to avoid misleading results.

The lower frame of figure 6.2 shows the received solar power by the radar Den Helder together with the reference values from DRAO. Before the annual maintenance the power from the DRAO monitoring station and the received solar power by Den Helder agree within 1 dB. During the maintenance the signal generator for the daily calibration of the logarithmic receiver was re-installed. In the first days after 6 April the solar power observed by the radar receiver is far from constant. After a week the received solar power has stabilized but unfortunately it has dropped by roughly 3 dB. The cause for this calibration difference has not been found yet.

Chapter 7

Conclusions

The radio frequency radiation emitted by the sun can be used to quantitatively monitor the elevation and azimuth alignment of a radar antenna and the sensitivity of a radar receiver. This is even more true for a weather radar network where the solar monitoring results for different radars can be compared. The solar interferences can be detected automatically in the polar reflectivity data produced operationally by an on-line weather radar using a straightforward procedure. For each detected solar interference the antenna elevation and azimuth, received power, and time stamp should be stored. The equations for the calculation of the position of the sun have been introduced and a way to obtain the current flux of radio frequency radiation from the sun has been put forward. Using a linear model the collected solar interferences can be analyzed quantitatively, and thus the biases of the elevation and azimuth reading of the radar antenna and the received solar power can be extracted. The potential of the sun for quantitatively monitoring of the alignment and performance of operational weather radars is clearly demonstrated by the two cases discussed in the last chapter. The results from the daily analysis of the solar interferences detected by the radars are available on the KNMI intranet:

`info.knmi.nl/~holleman/solarmonitor.html`

It is strongly recommended that this "solar monitor" is consulted by the radar maintenance staff on a daily basis.

Acknowledgments

Asko Huuskonen (FMI) is gratefully acknowledged for sharing experiences and interesting discussions. The authors thank Sylvia Barlag for supporting this unforeseen project and Wiel Wauben for carefully reviewing the manuscript.

References

Carroll, B. W. and D. A. Ostlie: 1996, *An Introduction to Modern Astrophysics*. Addison-Wesley Publishing Company, New York.

Crum, T.: 2001, WSR-88D Calibration: Changes and new Approaches. *Workshop on Radar Calibration, Albuquerque NM*, AMS.

Darlington, T., M. Kitchen, J. Sugier, and J. d. Rohan-Truba: 2003, Automated Real-time Monitoring of Radar Sensitivity and Antenna Pointing Accuracy. *31st conference on Radar Meteorology*, AMS, 538–541.

Doviak, R. J. and D. S. Zrnić: 1993, *Doppler Radar and Weather Observations*. Academic Press, second edition, 562 pp.

Gematronik: 2003, Rainbow 3.4 Operator's Manual. Gematronik GmbH., Raiffeneisenstr. 10, 41470 Neuss, Germany.

Holton, J. R.: 1992, *An introduction to dynamic meteorology*. Academic Press, third edition.

Huuskonen, A. and H. Hohti: 2004, Using the solar flux data from operational scans for checking the elevation pointing of a radar. *3rd European Conference of Radar Meteorology and Hydrology (ERAD)*, EMS.

Keeler, R. J.: 2001, Weather Radar Calibration. *Workshop on Radar Calibration, Albuquerque NM*, AMS.

Press, W. H., S. A. Teukolsky, W. T. Vetterling, and B. P. Flannery: 1992, *Numerical Recipes in C: the Art of Scientific Computing*. Cambridge University Press, second edition, 994 pp.

Rinehart, R.: 2001, Antenna Measurements: Dihedrals ground targets and antenna beam patterns. *Workshop on Radar Calibration, Albuquerque NM*, AMS.

SIGMET: 1998, RVP6 Doppler Signal Processor User's Manual. Sigmet, 2 Park Drive, Westford, MA 01886 USA.

Smith, P.: 2001, Basic Concepts of Weather Radar System Calibration and Performance Monitoring. *Workshop on Radar Calibration, Albuquerque NM*, AMS.

Sonntag, D.: 1989, *Formeln verschiedenen Genauigkeitsgrades zur Berechnung der Sonnenkoordinaten*. Abhandlungen des Meteorologischen Dienstes der DDR, no. 143, Akademie-Verlag, Berlin.

Tapping, K.: 2001, Antenna Calibration Using the 10.7cm Solar Flux. *Workshop on Radar Calibration, Albuquerque NM*, AMS.

WMO: 1996, *Guide to Meteorological Instruments and Methods of Observation, No. 8*. Secretariat WMO, Geneva, Switzerland, sixth edition.